Available online at www.sciencedirect.com
ScienceDirect
Journal of Catalysis 245 (2007) 308–315
JOURNAL OF CATALYSIS
www.elsevier.com/locate/jcat

Spectroscopic features and reactivity of CO adsorbed on different Au/CeO_2 catalysts

Maela Manzoli [a], Flora Boccuzzi [a,*], Anna Chiorino [a], Floriana Vindigni [a], Weiling Deng [b], Maria Flytzani-Stephanopoulos [b,*]

[a] *Dipartimento di Chimica IFM and NIS Centre of Excellence, Università di Torino, Torino, Via Pietro Giuria 7, 10125, Italy*
[b] *Department of Chemical and Biological Engineering, Tufts University, Medford, MA 02155, USA*

Received 13 September 2006; revised 23 October 2006; accepted 24 October 2006

Available online 28 November 2006

Abstract

An FTIR study of CO adsorption from 120 K up to room temperature on a series of Au–ceria samples is presented. Samples with low gold content (0.7 and 0.6 at%) were prepared by urea gelation/co-precipitation and by cyanide leaching of the high-gold content (5.8 at%) material prepared by deposition–precipitation on La-doped CeO_2. The samples were subjected to different pretreatments to collect information on the surface composition under working conditions. An absorption band at 2130–2140 cm^{-1}, not reversible on outgassing and more resistant to oxidation than the usual carbonyl band on Au^0 sites, was present due to CO adsorbed on cationic gold clusters. This highly stable species is relevant for hydrogen gas upgrade by removing CO from reformate-type gases at low temperatures. In addition, a broad absorption band in the 2000–2100 cm^{-1} range was observed after reduction in hydrogen, due to structural and electronic changes of gold. Interestingly, the reduced gold species in ceria can be reoxidized at mild conditions. Light-off of the CO oxidation reaction took place below room temperature on the metallic gold-containing ceria but was delayed until 310 K on the ionic gold-containing sample. TPR and XPS analysis of the fresh and used catalysts corroborated the stability of ionic gold in ceria up to 393 K in the reaction gas mixture.

Keywords: Gold–ceria catalysts; Gold ions; FTIR; CO adsorption; CO oxidation; XPS; TPR

1. Introduction

In recent years, many experimental and theoretical studies have attempted to understand the origin of the high activity of gold catalysts for different oxidation reactions at low temperatures, such as CO oxidation, CO-preferential oxidation (PROX) in H_2-rich gas streams, and the water–gas shift reaction (WGSR). Up to now, no unifying conclusions that account for all the observations have been available in the literature. Metallic gold (two atomic layers thick) deposited on a reducible oxide, such as titania, is proposed to have the highest activity in CO oxidation [1,2]. In this case, the gold surface sites are partially negatively charged, in agreement with the high electronegativity of gold. Other studies have provided evidence that gold cations, in the absence of metallic Au, exhibit high catalytic activity for the same reaction [3]. Fu et al. [4,5], in examining the WGSR on Au–ceria catalysts, found that cationic gold species strongly bound to ceria, Au_n–O–Ce, are the catalytically relevant species, and that the coexisting metallic gold nanoparticles do not participate in the reaction, as demonstrated by the same activity measured for cyanide-leached samples devoid of gold nanoparticles. A recent DFT calculation on the origin and activity of oxidized gold in WGSR [6] showed that the presence of empty localized nonbonding f states in CeO_2 permits the oxidation of Au, allowing stronger CO chemisorption. The conclusion was that the active sites of Au/CeO_2 for the WGSR are ultrasmall Au clusters bearing a positive charge and localized near an oxygen vacancy of ceria. Finally, although without direct evidence, it has been proposed [7] that the active sites in Au/TiO_2 for the CO oxidation reaction include both metallic gold and Au cations at the perimeter of the gold

* Corresponding authors.
E-mail addresses: flora.boccuzzi@unito.it (F. Boccuzzi), mflytzan@tufts.edu (M. Flytzani-Stephanopoulos).

0021-9517/$ – see front matter
doi:10.1016/j.jcat.2006.10.021

Table 1
Physicochemical properties of gold–ceria materials[a]

Sample	BET SA (m^2/g)	Surface composition[b] (at%)			Bulk composition[c] (at%)			Crystallite size[d] CeO_2 (nm)	
		Au	Ce	La	Au	Ce	La	⟨111⟩	⟨220⟩
5.8AuCL(DP)	164.9	2.19	78.90	18.91	5.83	86.48	7.68	6.0	7.1
0.6AuCL(DP,NaCN)	160.9	0.26	80.67	19.07	0.57	92.03	7.40	5.6	6.8
$0.7AuCeO_2$ (UGC)	170.1	0.28	99.72	0	0.69	99.31	–	5.0	6.2
CeO_2 (UGC)	140.5	–	–	–	–	100	–	7.1	6.6

[a] All samples were calcined at 673 K in air for 10 h, except the leached samples for 2 h.
[b] Surface composition was determined by XPS.
[c] Bulk composition was determined by inductively coupled plasma (ICP) emission spectrometry.
[d] The crystallite size was determined from XRD data with the Scherrer equation.

nanoparticles with the oxide support. All of these apparently conflicting results may be rationalized by taking into account that pretreatments, preparation methods, and reaction mixture compositions can influence the nature of the exposed gold sites and their catalytic activities.

Among the different gold-oxide preparation techniques and pretreatments, the deposition–precipitation method followed by activation via calcination in air at 673 K is widely used to disperse gold nanoparticles on oxidic supports. However, recent reports have noted that other kinds of activation, such as reduction with hydrogen or CO, may be more efficient [8] in producing ultrafine (∼2 nm) gold particles on titania active for the CO oxidation reaction. On the other hand, for the Au–CeO_2 system, air calcination is better for stable WGSR activity, as is sample preparation by one-pot gelation/coprecipitation with urea decomposition [5]. Surface reduction by hydrogen may of course occur directly in the PROX and in the WGS reactions mixtures at certain temperatures.

In this work, we used FTIR spectroscopy to follow the various states of CO adsorbed on different Au/CeO_2 catalysts prepared at Tufts University. CO adsorption spectra at different temperatures on the as-prepared and leached samples subjected to different pretreatments were examined to obtain direct information on the surface composition of the catalysts under some working conditions. Catalytic results and TPR and XPS analysis of these materials complement the FTIR studies.

2. Experimental

2.1. Materials

Gold–ceria samples were prepared by deposition precipitation (DP) and by one-pot synthesis by the urea gelation/coprecipitation (UGC) method, as described in detail elsewhere [5,9]. Lanthana-doped ceria and undoped ceria supports also were prepared by the UGC method [9].

A 5.8 at% gold catalyst supported on lanthana-doped ceria (hereafter referred as 5.8AuCL) was subjected to a cyanide leaching process in an aqueous solution of 2% NaCN under O_2 gas sparging at room temperature (r.t.) and high pH (12). Leaching removed about 90% of the gold from the parent 5.8AuCL sample, resulting in a sample containing 0.6 at% of gold (0.6AuCL). No cerium or lanthanum was found in the leachate checked by ICP. Finally, a sample prepared by the UGC method without added lanthanum and containing almost the same amount of gold (0.7 at%) as 0.6AuCL was also examined ($0.7AuCeO_2$). For comparison, the support alone (CeO_2) prepared by the same UGC procedure was considered. All samples but one were calcined in air at 673 K for 10 h; the leached sample was calcined for 2 h. A slow heating rate of 2 K/min up to the final calcination temperature was used. The physical and chemical properties of the catalyst samples examined in this work are shown in Table 1.

2.2. FTIR measurements

The FTIR spectra were collected on a Perkin-Elmer 1760 spectrometer (equipped with a MCT detector), with the samples in self-supporting pellets introduced in a cell, allowing thermal treatment in controlled atmospheres and spectrum scanning at controlled temperatures (from 120 K up to room temperature). All the spectra were collected in static conditions at the indicated pressure and temperature. The FTIR cell was connected through a needle valve to a VGQ Thermo ONIX spectrometer equipped with a Thoria filament and a Faraday detector, to obtain the analysis of the gas phase. The gas-phase composition of the different initial gas mixtures and during reaction was determined by recording the mass spectrum, using a leak valve set to maintain a 10^{-6} mbar pressure in the detection chamber.

2.2.1. Pretreatments before the spectroscopic measurements

The catalyst samples were subjected to the following pretreatments:

- Outgassing at room temperature (as received catalysts); all samples.
- For the reduced samples, outgassing was followed by three cycles of reduction in H_2, up to 373 K, or up to 473 K.

2.3. CO oxidation reaction

CO oxidation reaction tests were conducted at atmospheric pressure with the catalyst in powder form (<150 μm). A quartz tube (1 cm o.d.) with a porous quartz frit supporting the catalyst was used as a packed-bed flow reactor. The feed and product gas streams were analyzed using a HP-6890 gas chromatograph (GC) equipped with a thermal conductivity detector (TCD). The inlet gas composition was 0.8% CO, 0.4% O_2, and balance helium, and the space velocity was 60,000 h^{-1}. The reactant gases

CO and O_2, in a certified calibration gas mixture with helium (Airgas), were measured by mass flow controllers and mixed before the reactor inlet. The reaction temperature was controlled with an Omega temperature controller. Steady-state CO conversion data were collected from room temperature to 393 K (ascending temperature mode). No hysteresis was present, as verified by repeating measurements at low temperatures after completion of the test at 393 K.

2.4. Other characterization techniques

Temperature-programmed reduction by hydrogen (H_2-TPR) was conducted in a Micromeritics Pulse ChemiSorb 2705 instrument equipped with a thermal conductivity detector to measure H_2 consumption. Samples were purged in helium at room temperature for 0.5 h before each test, then heated at a rate of 5 K/min from room temperature to 673 K in a 20% H_2/N_2 [50 cm^3/min (STP)]. A Kratos AXIS ultra imaging X-ray photoelectron spectrometer (XPS) with a resolution of 0.1 eV was used to determine the atomic metal ratios of the surface region and the oxidation state of gold in selected catalysts. Samples in powder form were pressed on a double-sided adhesive copper tape for analysis. An AlK_α X-ray source was used in this work. All binding energies were adjusted by using C1s as internal standard. XRD analysis was performed on a Rigaku 300 instrument with a rotating anode generator and a monochromatic detector. CuK_α radiation was used with power settings of 60 kV and 300 mA. TOPAS software (Bruker) was used to perform microstructure analysis.

3. Results and discussion

3.1. As-received catalysts

As-received samples were simply outgassed at room temperature. Fig. 1a shows the FTIR spectra on the as-received 5.8AuCL sample after CO adsorption at 120 K and after heating in CO to room temperature Fig. 1b shows the spectra of a second adsorption of CO on the same sample, now reduced in CO and cooled again to 120 K. Similar experiments performed on 0.6AuCL are shown in Fig. 2.

After CO adsorption at 120 K on the as-received 5.8AuCL sample (Fig. 1a, bold curve) a band at 2100 cm^{-1}, almost unperturbed by the temperature increase and assigned to CO adsorbed on Au^0 step sites on small particles [10] and a strong band at 2160 cm^{-1}, closely related to the band observed on pure CeO_2 (not shown here for the sake of brevity) that smoothly reduces in intensity as temperature increases, due to CO adsorbed on Ce^{4+} sites [11], are observed. The same experiment performed on the 0.6AuCL sample (Fig. 2, dotted curve) produced only the band centered at 2160 cm^{-1}, because no gold particles were present on this sample after leaching with NaCN.

During the heating to room temperature, a broad absorption with a maximum at 2130–2140 cm^{-1} appears (bold dashed curve). After the second adsorption of CO at 120 K, some significant differences are evident on both samples. In particular, starting from 5.8AuCL, the comparison between the as-received sample and the one reduced in CO (bold curves of Figs. 1a and 1b) clearly shows the intensification of the band at 2100 cm^{-1}, the increase of the broad absorption at 2130–2140 cm^{-1}, the decrease of the intensity of the band

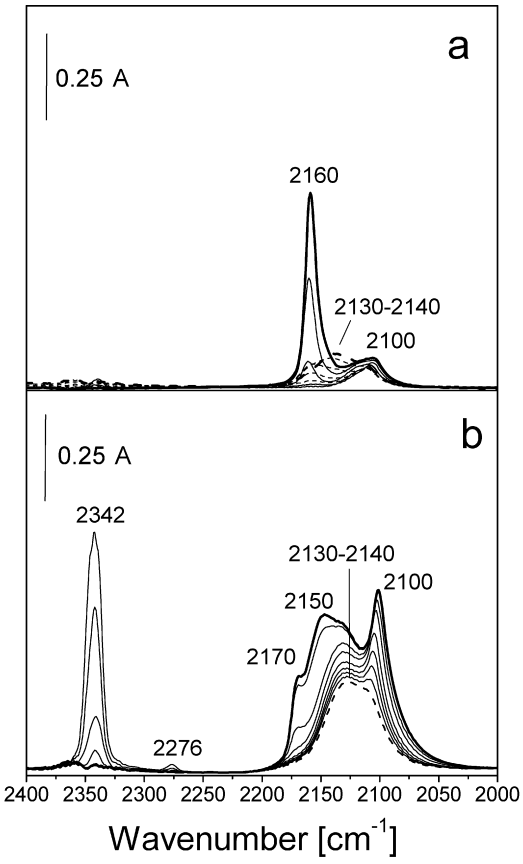

Fig. 1. (a) FTIR spectra after the interaction with 0.5 mbar CO at 120 K on the as received 5.8AuCL sample (—) and during the heating (—, - - -, successively) up to r.t. (– – –). (b) FTIR spectra after a second interaction with 0.5 mbar CO at 120 K on the same 5.8AuCL sample previously contacted with CO (—) and during the heating (—) up to r.t. (- - -).

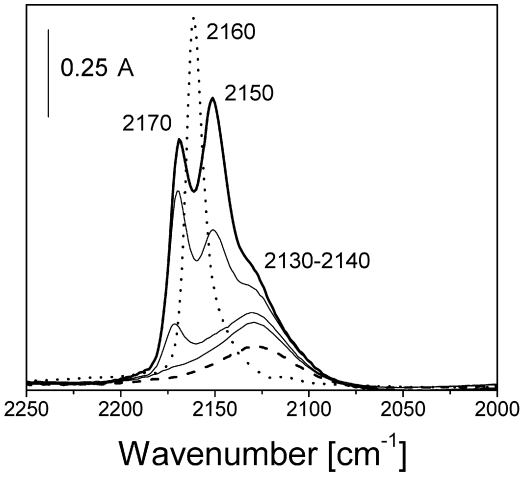

Fig. 2. FTIR spectra after the interaction with 0.5 mbar CO at 120 K on the as received 0.6AuCL sample (···) and after a second interaction with 0.5 mbar CO at 120 K on the same 0.6AuCL sample previously contacted with CO (—) and during the heating (—) up to r.t. (- - -).

at 2160 cm^{-1} and the appearance of a new component at 2170 cm^{-1}. Moreover, a strong band at 2342 cm^{-1} is seen, due to asymmetric stretching of molecular CO_2 [12], not observed in the first interaction.

The intensification of the band at 2100 cm^{-1} is an indication that most of the gold sites are covered by adsorbed oxygen. This could be a consequence of the presence, on the as-received sample, of a large number of Au nanoparticles of very small size. It has already been shown on other gold samples that gold particles smaller than 2 nm remain oxidized [1,2,12]. This may explain the larger amount of clean gold sites seen after reaction of CO with oxygen, as also indicated by the production of CO_2 during heating in CO (Fig. 1b).

The broad and strong band in the 2130–2140 cm^{-1} range remaining after heating to room temperature in 0.5 mbar of CO (Fig. 1b, dashed curve), has a position similar to that produced on the as-received sample during the heating to room temperature (Fig. 1a, bold dashed curve). The higher resistance to the outgassing and the blue shift with respect to the usual frequency of CO on metallic gold sites indicates that the adsorption sites are positively charged. It is known that the bonding of CO to positively charged Au, Cu, and Ag sites is stronger than on the respective metallic sites [13]. This is due to the change in the nature of the bonding due to the effect of the increase of the σ bond and of the synergistic increase of the π back-bond. These facts produce a blue shift of the CO stretching frequency and an increase in overall $Au^{\delta+}$–CO strength. Similar features have been previously observed only on highly dehydrated Au/TiO_2 [14]. In contrast, this feature was not detected on other gold catalysts submitted to similar pretreatments and experiments to those used here (e.g., Au/Fe_2O_3 and Au/TiO_2 reference catalysts provided by the World Gold Council) [15]. Wu et al. [16] used DFT to calculate the IR frequencies of carbon monoxide adsorbed on small gold clusters. They reported greater adsorption energies of CO on the cationic clusters than those on the neutral and anionic complexes. Moreover, the calculated CO vibrational frequencies were larger than on neutral clusters. Based on these findings, as well as on other experimental data [3,17], it can be proposed that the absorption band in the 2130–2140 cm^{-1} range is related to CO adsorbed on small cationic gold clusters, like $Au_n(CO)_m^+$, with $4 \leqslant n \leqslant 6$ [18]. The increased intensity of this absorption after reduction in CO is an indication that the small cationic gold clusters are also initially covered by adsorbed oxygen and probably are in a higher oxidized state.

It must be stressed that gold in the 5.8AuCL sample discussed here is supported on a La-doped ceria. This kind of doping may induce a large number of oxygen vacancies where gold clusters can nucleate [4,5]. Finally, the band at 2170 cm^{-1}, not observed during the first interaction with CO at 120 K (section a, bold curve), is assigned to coordinatively unsaturated (cus) Ce^{4+} sites [19], possibly close to the gold clusters and created after the first CO adsorption by the reactive interaction of CO with the surface Ce–O species from 120 K up to room temperature.

The initial 120-K spectrum of CO over the 0.6AuCL leached sample (Fig. 2, dotted curve) is totally modified after heating in CO up to room temperature and successive cooling again to 120 K (Fig. 2, bold curve). The main features are the formation of the band at 2170 cm^{-1} on Ce^{4+} (cus) already discussed, an intense but weakly resistant band at 2150 cm^{-1} related to CO coordinated to the water condensed at the surface of the catalyst after the second cooling [13], and a band at 2130–2140 cm^{-1} due to adsorption of CO on small cationic gold clusters. We also observed very similar spectroscopic features on the $0.7AuCeO_2$ catalyst prepared by the UGC method and subjected to the same treatment (not shown); only a lower intensity absorption in the band at 2130–2140 cm^{-1} was seen. Thus, the 2100-cm^{-1} band is still absent in these samples; no carbonyls on metallic gold nanoparticles are seen, even after heating in CO up to room temperature.

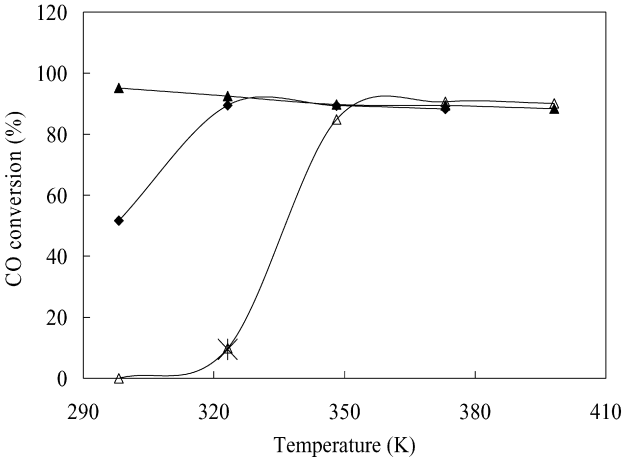

Fig. 3. CO oxidation light-off over gold–ceria catalysts in ascending temperature mode and after steady-state was reached at each temperature. (▲) 5.8AuCL; (△) 0.6AuCL; (◆) 0.6AuCL pretreated in hydrogen at 473 K; (✳) 0.6AuCL, after cooling down to 323 K following steady-state testing at 393 K. Gas mixture: 0.8% CO–0.4% O_2–He; $W/F = 0.12$ g s/cc.

Finally, FTIR spectra combined with quadrupole mass spectrometry (QMS) data were collected on the samples outgassed at room temperature for which only the band at 2130–2140 cm^{-1} was present. In the absence of the gas phase, the intensity of absorption was retained almost completely up to 373 K, whereas it was totally depleted at 423 K (data not shown). With heating in the presence of O_2 (10 mbar), the band was almost completely depleted already at 373 K; thus, the CO adsorbed on cationic gold sites starts to react with oxygen below this temperature. As for the mass spectrum, in addition to the peaks related to the presence of an excess of oxygen, new peaks at $m/z = 16$, 28, and 44 related to CO_2 were also observed. The temperature of the reaction of adsorbed CO with oxygen is very close to the temperature at which catalytic PROX tests were previously performed on these samples by some of us [20].

In this work, we examined the activity of the different gold species on ceria in the stoichiometric CO oxidation reaction. The light-off curves shown in Fig. 3 can be correlated with the different reactivity of Au^0 and $Au^{\delta+}$ for CO oxidation. Au^0 and $Au^{\delta+}$ both adsorb CO with different strengths, as discussed above, and they react with oxygen to produce CO_2, but in different temperature windows. The 0.6AuCL sample, which

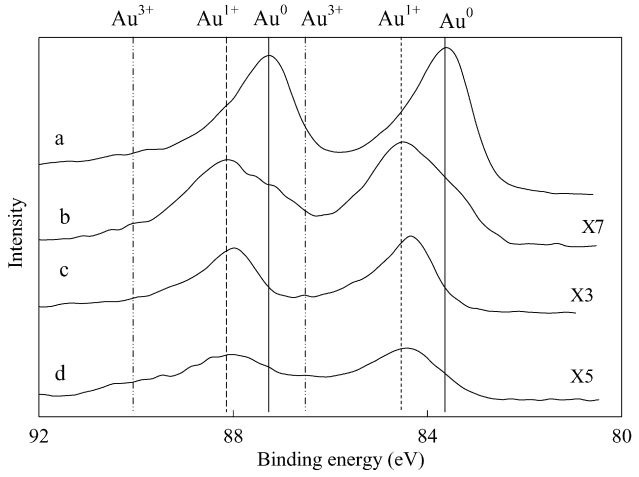

Fig. 4. XPS (Au4f spectra) characterization of gold–ceria samples. (a) 5.8 AuCL; (b) 0.6AuCL; (c) used 0.6AuCL after CO oxidation at 393 K; (d) 0.7Au-CeO_2. X7, X3, X5 represent the signal magnification.

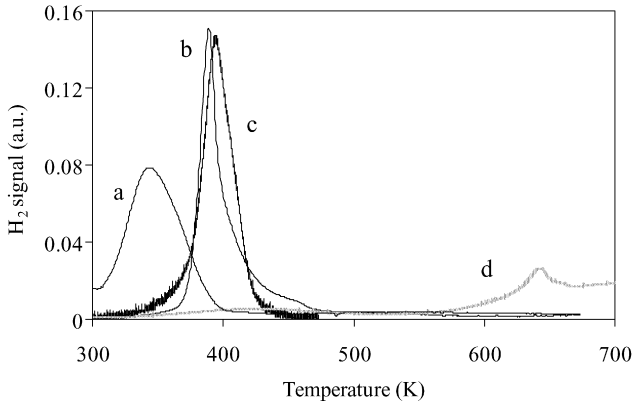

Fig. 5. H_2-TPR of 5.8AuCL and 0.6AuCL samples. (a) Fresh 5.8AuCL; (b) fresh 0.6AuCL; (c) 0.6AuCL after use in CO oxidation reaction at 393 K at the conditions of Fig. 3; (d) CL, i.e. Ce(10% La)O_x, all samples were purged in He at 298 K before heating in 20% H_2/N_2 50 cc/min; heating rate 5 K/min.

contains mainly oxidized gold species as identified by XPS in Fig. 4, by FTIR in Fig. 2, and by H_2-TPR in Fig. 5, has a much higher light-off temperature than the 5.8AuCL sample (containing gold nanoparticles), which lights-off below room temperature. The reaction light-off on the 0.6AuCL sample is at ∼310 K, the temperature at which FTIR and QMS data indicate that CO adsorbed on cationic gold starts to be oxidized. No hysteresis was observed when the CO conversion data were collected in descending temperature, after the steady-state test at 393 K. Thus, in this reaction mixture, ionic gold is not reduced up to 393 K.

XP Au4f spectra are shown in Fig. 4 for the various catalysts examined in this work. Au^0 is present in the 5.8AuCL sample (line a), whereas the 0.6AuCL and 0.7AuCeO$_2$ (lines b and d), respectively, contain cationic gold, principally Au^+. The reaction used 0.6AuCL sample after the test at 393 K (line c) shows the presence of cationic gold, similar to the fresh catalyst.

H_2-TPR was also used to characterize the gold-ceria samples. As can be seen in Fig. 5, the fresh 0.6AuCL sample containing cationic gold as found by XPS is well bound to ceria, with surface oxygen starting to decrease above 373 K (line b) [20,21]. The used catalyst after reaction at 393 K was also characterized by H_2-TPR (line c in Fig. 5); the profile was almost the same as that for the fresh material, indicating that the gold oxidation state remained the same. If Au^0 nanoparticles had been formed during reaction, then the reduction of the ceria surface oxygen would have shifted to a lower temperature [21], as was the case for 5.8AuCL (the H_2-TPR of which is shown in Fig. 5, line a). For comparison, the TPR of the support CL (Ce(10% La)O_x) is also shown in this figure (line d).

The 0.6AuCL catalyst was treated in 20% H_2–He gas mixture up to 473 K at a heating rate of 5 K/min and maintained at 473 K for 2 h. The CO oxidation reaction light-off curve on the thus-treated material is shown in Fig. 3. Clearly, this is now much more active than the fresh 0.6AuCL, which is composed of cationic gold only.

In conclusion, all of the foregoing tests have demonstrated that Au^0 species are much more active for dry CO oxidation than positively charged gold species, which, as shown in the FTIR data of Fig. 2, bind CO more strongly than Au^0.

3.2. *Catalysts reduced in H_2*

The spectroscopic features related to CO adsorption on reduced Au-CeO_x catalysts are of interest, because they may apply to high-temperature CO oxidation, the PROX reaction, and others. Figs. 6 and 7 show FTIR spectra collected on pre-reduced catalysts. At 120 K on the 5.8AuCL sample, reduced in hydrogen at 373 K (not shown) and at 473 K (Fig. 6a, bold curve) the spectra essentially overlap, whereas they are quite different than those observed on the same sample reduced in CO at room temperature (bold curve in Fig. 1b). In particular, the band at 2100 cm^{-1}, due to CO adsorbed on Au^0, and that at 2130–2140 cm^{-1}, assigned to CO interacting with Au_n^+ clusters, are both missing. The bands at 2140 cm^{-1} and at 2163 cm^{-1}, related to "liquid-like" CO [19] and to CO adsorbed on cationic Ce^{x+} sites [19], respectively, are shown in Fig. 6a. Moreover, a broad absorption band with a maximum at 2085 cm^{-1} extending from 2100 to 1950 cm^{-1} is now produced (Fig. 6a, bold curve). This feature has not been observed on gold catalysts supported on other oxides, as, for example, the reference gold catalysts supported on TiO_2 or Fe_2O_3 and reduced at even higher temperatures [14]. On the other hand, the absorption band observed here has been previously observed on other Au/CeO_2 catalysts [22]. It should be noted that species irreversible to the outgassing at room temperature were detected on fresh and freshly reduced Au/TiO_2 and Au/Fe_2O_3 at 2055 and at 1990 cm^{-1} [23]. These bands, on the basis of their behavior at decreasing CO pressures, were assigned to CO linearly adsorbed on top and bridge-bonded, respectively, on small gold clusters, negatively charged. However, these bands disappeared in successive interactions, possibly as a consequence of coalescence of gold clusters into larger particles. In contrast, this low-frequency band is still present on reduced Au/CeO_2 after many redox treatments.

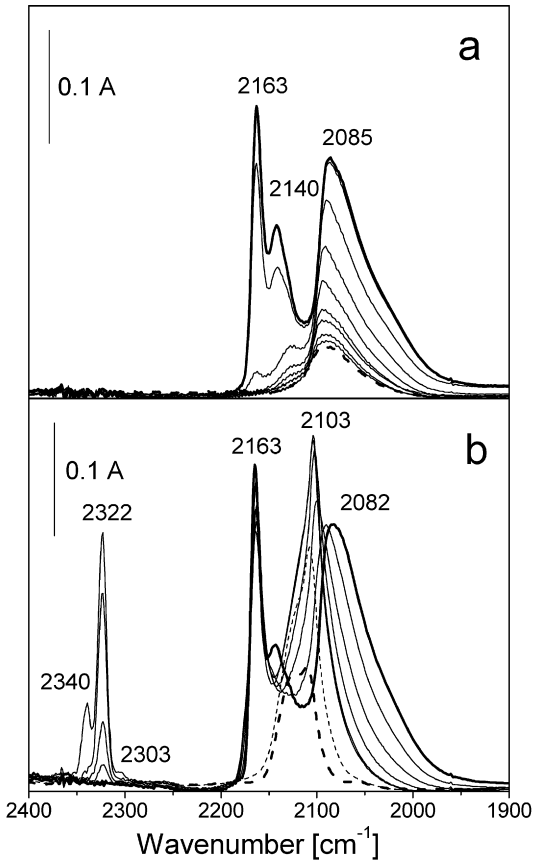

Fig. 6. (a) FTIR spectra after the interaction with 0.5 mbar CO at 120 K on the 5.8AuCL sample reduced in H_2 at 473 K (—) and during heating in CO (—) up to r.t. (- - -). (b) FTIR spectra after the interaction with 0.5 mbar CO at 120 K on the 5.8AuCL sample reduced in H_2 at 473 K (—), after the introduction of 0.5 mbar $^{18}O_2$ at 120 K and with increasing diffusion times at the same temperature (—) and during heating (- - -) up to r.t. (– – –) in the CO–$^{18}O_2$ mixture.

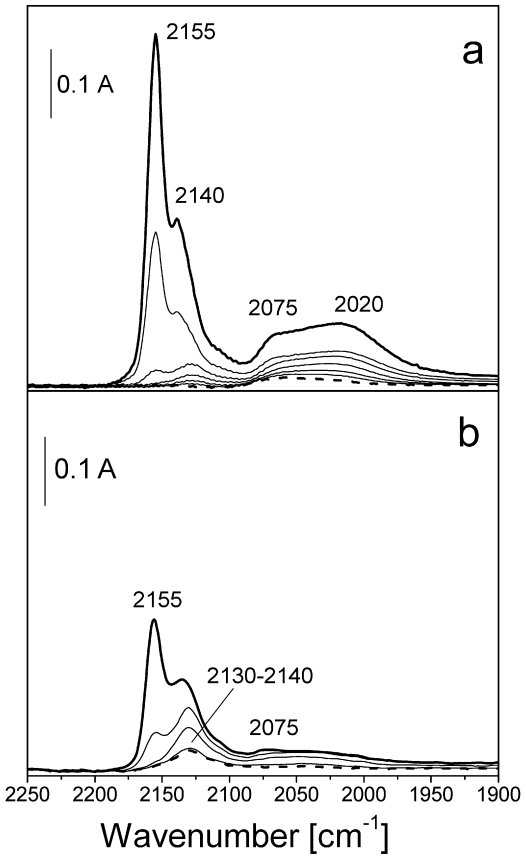

Fig. 7. (a) FTIR spectra after the interaction with 0.5 mbar CO at 120 K on the 0.6AuCL sample reduced in H_2 at 473 K (—) and during the heating in CO (—) up to r.t. (- - -). (b) FTIR spectra after the interaction with 0.5 mbar CO at 120 K on the 0.7AuCeO$_2$ sample reduced in H_2 at 473 K (—) and during the heating in CO (—) up to r.t. (- - -).

It appears that the adhesion and the wetting of gold particles on reduced ceria and La-doped ceria increase compared with the untreated ones, different from what is found on other supports. Potentially, after reduction, Au spreads on the reduced ceria, and three-dimensional gold nanoparticles may become very thin films. This is in line with recent in situ HRTEM observations of gold–ceria interaction reported by Akita et al. [24]. These authors chose a "model" ceria exposing low-index flat faces, typically the {111} and {100} planes, to facilitate observation, because due to poor contrast, it is very hard to observe gold particles on ceria nanoparticles. They found that under the beam and in vacuum, the smallest and thin gold nanoparticles disappeared, shrinking layer by layer down to a monatomic layer. A similar phenomenon also may occur by reducing the 5.8AuCL sample in H_2 at 473 K. Metal spreading was observed for the first time by in situ HRTEM for Cu/ZnO catalysts in a reducing reaction atmosphere [25]. It must be emphasized that on other gold catalysts supported on reducible oxides and reduced in hydrogen, only the usual absorption band of CO on gold sites at ∼2100 cm^{-1} is seen even after reduction in hydrogen at 523 K [26], without any significant red shift.

Isotopic experiments with $^{18}O_2$ were conducted to investigate the CO reactivity. The introduction of $^{18}O_2$ at 120 K and with increasing diffusion times at the same temperature (Fig. 6b, fine curves) over the 5.8AuCL sample reduced at 373 K and previously saturated by CO at 120 K (bold curve), produces immediately a strong erosion from the low-frequency side of the band at 2087 cm^{-1}. After the $^{18}O_2$ interaction at 120 K, the band shifts from 2087 cm^{-1} up to 2103 cm^{-1} and it appears narrow and with a maximum in the usual position of CO adsorbed on Au^0 sites, while at the same time a shoulder at 2120 cm^{-1} is produced. Moreover, a strong and broad absorption at about 3190 cm^{-1} is seen, possibly related to OH groups formed by reaction between the oxygen and residual atomic hydrogen (not shown) [23,24]. In addition, a band at 2322 cm^{-1} related to C^{18}O^{16}O appears immediately, whereas bands at 2340 and 2303 cm^{-1}, related to C$^{16}O_2$ and C$^{18}O_2$, respectively, are produced over time, reaching their maximum intensity after a diffusion time of about 20 min. With heating to room temperature (Fig. 6b, bold dashed curve) in the same mixture, the bands at 2103 cm^{-1} and at 2160 cm^{-1} are reduced in intensity and depleted, similar to what is observed for the absorption related to the isotopomers of CO_2. Moreover, a residual absorption band at 2130–2140 cm^{-1} is produced, very similar to that already observed on this sample after heat-

ing to room temperature in CO (Fig. 1b, dashed curve). These features provide strong evidence that negatively charged gold clusters are converted into positively charged ones by oxidation.

Therefore, FTIR data show that in oxidizing conditions, the CO interaction with the gold–ceria samples produces absorption bands in the region typical for cationic gold clusters (see Figs. 1b and 2a), whereas in reducing conditions, zerovalent gold clusters are produced, possibly negatively charged by strong interaction with reduced ceria and characterized by a CO IR signature red-shifted to below 2100 cm^{-1} (see Fig. 6a). Oxidation restores the surface stoichiometry of the ceria and the usual position of adsorbed CO.

Here we do not show the spectra obtained after CO adsorption at 120 K on 0.6AuCL and 0.7$AuCeO_2$ reduced in hydrogen at 373 K, because the results are in both cases similar to those obtained on the 0.6AuCL reduced in CO (bold curve in Fig. 2a), the main difference being the significantly larger intensity of the 2170 cm^{-1} band, assigned to Ce^{4+} cus sites. However, prereduction of the low-content gold samples at 473 K does make a big difference. FTIR data from the CO adsorption experiments performed on the 0.6AuCL and 0.7$AuCeO_2$ samples, both reduced in H_2 at 473 K, are reported in Figs. 7a and 7b, respectively. Similar to the 5.8AuCL sample, CO was adsorbed at 120 K (bold curves of Figs. 7a and 7b), and the samples were maintained in the CO atmosphere at increasing temperature (fine curves) up to room temperature (dashed curve). In the higher frequency range of the carbonylic region reported in Fig. 7, bands related to "liquid-like" CO [19] and to CO adsorbed on cationic Ce^{x+} sites [19] are present on both samples. In the 2100–1950 cm^{-1} range, a broad absorption is observed. In the same frequency region, vibrational spectra of the carbonyl complexes of anionic gold clusters measured in the gas phase have been reported [27], similar to those observed previously by some of us [23]. However, the intensity of the bands at 2070 and 2020 cm^{-1} is significantly weaker on 0.7$AuCeO_2$ than on 0.6AuCL, and a residual band at 2130–2140 cm^{-1} is observed on the former during the heating in CO up to room temperature (dashed curve, section b). Both of these features indicate that ionic gold is less easily reduced on 0.7$AuCeO_2$, probably because on this sample, prepared by the one-pot gelation method, more gold is in solid solution with ceria [20]. Interestingly, as shown in Table 1, the XPS-measured surface concentration of gold on this sample and on the leached 0.6AuCL sample are similar, both values being much lower than the bulk gold content measured by ICP.

Looking at the same experiment in the full spectral range, in addition to the bands in the carbonylic region discussed earlier (Fig. 7), two intense peaks at 3697 and 3670 cm^{-1} and an absorption centered at 3220 cm^{-1} were observed after the introduction of CO at 120 K on the 0.6AuCL sample reduced at 473 K (Fig. 8, solid curve). These bands are related to OH groups of the support and produced after the introduction of CO at 120 K, because of the presence of hydrogen on the gold particles after the reduction step. CO is able to displace the hydrogen atoms that spill over onto the support producing the OH groups. These OH groups can reveal reduced Ce^{3+} sites near gold.

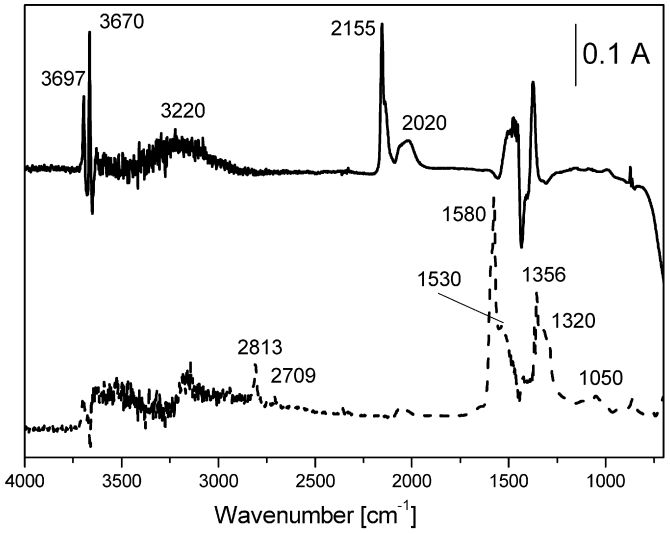

Fig. 8. FTIR spectra after the interaction with 1 mbar CO at 120 K on the 0.6AuCL sample reduced in H_2 at 473 K (—) and after the heating in CO up to r.t. (- - -).

By heating in a CO atmosphere to room temperature (dashed curve), the OH groups are totally depleted. At the same time, in the CH stretching region bands at 2813 and 2709 cm^{-1}, as well as at lower frequencies, bands related to monodentate and bidentate formate species, produced by the reaction between the CO molecules and the OH groups during the heating, are observed. The CO adsorbed on gold is also depleted, according to the data in Fig. 8. Similar behavior is also observed on the 5.8AuCL sample. In contrast, no growth of OH groups is detected on the 0.7$AuCeO_2$ catalyst (not shown). Therefore, a role for lanthanum doping in the formation of these reactive OH species may be inferred. However, we believe that further detailed studies of reactivity of the CO adsorbed on oxidized gold are needed to elucidate the mechanism of the water–gas shift reaction on gold–ceria catalysts.

4. Conclusions

Going back to the open questions posed in Section 1 about the role of the different gold oxidation states and of gold dispersion on the activity of gold catalysts, the main results obtained in the present work can be summarized as follows:

1. By conducting CO adsorption from 120 K to room temperature on different gold on La-doped and undoped ceria, we used FTIR to identify the presence of cationic gold species in strong interaction with ceria, the abundance of which depends on the preparation method (DP or UGC) and on the sample pretreatments. These cationic gold clusters, characterized by a maximum CO absorbance at 2130–2140 cm^{-1}, bind CO strongly up to ∼373 K, whereas CO is more weakly adsorbed on gold nanoparticles, readily reacting with oxygen already at room temperature.
2. The positively charged clusters evolve in the direction of negatively charged species in reducing atmospheres and back to positively charged species by interaction with oxy-

gen. This facile redox of gold on ceria is unusual. In reducing conditions, a red-shifted CO absorption band is observed, similar to that reported by Chen and Goodman on model Au/TiO_2 catalysts [1,2]; the trend is much more evident for the La-doped ceria catalysts. This is an intriguing result, taking into account that on other gold catalysts supported on reducible oxides and reduced in hydrogen, the usual absorption band at $\sim$2100 cm^{-1} assigned to CO bonded at the step sites of small gold particles also persists on the samples reduced in hydrogen at 523 K (i.e., Au/TiO_2 [12] and Au/ZnO [26]).

3. On gold–ceria catalysts, gold nucleates probably at oxygen defect sites of ceria and remains highly dispersed and in good contact with the support. The gold atoms directly in contact with ceria are positively charged and highly stable, as shown by the fact that they are not removed during the leaching step. Doping with La_2O_3 increases the number of oxygen defects in ceria, thus leading to a higher concentration of strongly bound gold atoms [4]. In a steady-state CO oxidation reaction at stoichiometric conditions at 393 K, these gold species remained positively charged and strongly bound to ceria. It will be interesting to follow the stability of these species in other reactions, such as the WGSR, where they have been reported to be active [4,5] and predicted by DFT calculations [6].

Acknowledgments

This work was supported by MIUR–PRIN 2004, INCA Interuniversity Consortium Chemistry for the Environment, the U.S. National Science Foundation (NIRT grant 0304515), and the U.S. Department of Energy (Basic Energy Sciences, Hydrogen Fuel Initiative grant DE-FG02-05ER15730).

References

[1] M.S. Chen, D.W. Goodman, Science 306 (2004) 5694.
[2] M.S. Chen, D.W. Goodman, Catal. Today 111 (2006) 22.
[3] J.C. Fierro-Gonzales, B. Gates, J. Phys. Chem. B 108 (2004) 16999.
[4] Q. Fu, H. Saltsburg, M. Flytzani-Stephanopoulos, Science 301 (2003) 935.
[5] Q. Fu, W. Deng, H. Saltsburg, M. Flytzani-Stephanopoulos, Appl. Catal. B 56 (2005) 57.
[6] Z.-P. Liu, S.J. Jenkins, D.A. King, Phys. Rev. Lett. 94 (2005) 196102.
[7] J.H. Yang, J.D. Henao, M.C. Raphulu, Y. Wang, T. Caputo, A.J. Groszek, M.C. Kung, M.S. Scurrell, J.T. Miller, H.H. Kung, J. Phys. Chem. B 109 (2005) 10319.
[8] B. Schumacher, V. Plzak, J. Cai, R. Behm, J. Catal. Lett. 101 (2005) 215.
[9] Q. Fu, A. Weber, M. Flytzani-Stephanopoulos, Catal. Lett. 77 (2001) 87.
[10] G.C. Bond, D.T. Thompson, Catal. Rev. Sci. Eng. 41 (1999) 319, and references therein.
[11] C. Li, Y. Sakata, T. Araï, K. Domen, K. Maruya, T. Onishi, J. Chem. Soc. Faraday Trans. I 85 (1989) 929.
[12] F. Boccuzzi, A. Chiorino, M. Manzoli, P. Lu, T. Akita, S. Ichikawa, M. Haruta, J. Catal. 202 (2001) 256.
[13] K.I. Hadjiivanov, G.N. Vayssilov, Adv. Catal. 47 (2002) 307, and references therein.
[14] F. Boccuzzi, A. Chiorino, S. Tsubota, M. Haruta, J. Phys. Chem. 100 (1996) 3625.
[15] F. Menegazzo, M. Manzoli, A. Chiorino, F. Boccuzzi, T. Tabakova, M. Signoretto, F. Pinna, N. Pernicone, J. Catal. 237 (2006) 431.
[16] X. Wu, L. Senapati, S.K. Nayak, A. Selloni, M. Hajaligol, J. Chem. Phys. 117 (2002) 4010.
[17] J. Guzman, S. Carrettin, A. Corma, J. Am. Chem. Soc. 127 (2005) 3286.
[18] A. Fielicke, G. von Helden, G. Meijer, D.B. Pedersen, B. Simard, D.M. Rayner, J. Am. Chem. Soc. 127 (2005) 8416.
[19] C. Binet, M. Daturi, J.C. Lavalley, Catal. Today 50 (1999) 207.
[20] W. Deng, J. De Jesus, H. Saltsburg, M. Flytzani-Stephanopoulos, Appl. Catal. A 291 (2005) 126.
[21] Q. Fu, S. Kudriavtseva, H. Saltsburg, M. Flytzani-Stephanopoulos, Chem. Eng. J. 93 (2003) 41.
[22] T. Tabakova, F. Boccuzzi, M. Manzoli, D. Andreeva, Appl. Catal. A 252 (2003) 385.
[23] F. Boccuzzi, A. Chiorino, M. Manzoli, D. Andreeva, T. Tabakova, J. Catal. 188 (1999) 176.
[24] T. Akita, M. Okumura, K. Tanaka, M. Kohyama, M. Haruta, J. Mater. Sci. 40 (2005) 3101.
[25] P.L. Hansen, J.B. Wagner, S. Helveg, J.R. Rostrup-Nielsen, B.S. Clausen, H. Topsøe, Science 295 (2002) 2053.
[26] M. Manzoli, A. Chiorino, F. Boccuzzi, Appl. Catal. B 52 (2004) 259.
[27] A. Fielicke, G. von Helden, G. Meijer, B. Simard, D.M. Rayner, J. Phys. Chem. B 109 (2005) 23935.